Original Articles

A new remote sensing index for assessing the spatial heterogeneity in urban ecological quality: A case from Fuzhou City, China

Xisheng Hu[a,b,c,d], Hanqiu Xu[a,c,d,*]

[a] College of Environment and Resources, Fuzhou University, Fuzhou, Fujian 350108, China
[b] College of Transportation and Civil Engineering, Fujian Agriculture and Forestry University, Fuzhou, Fujian 350002, China
[c] Institute of Remote Sensing Information Engineering, Fuzhou University, Fuzhou, Fujian 350108, China
[d] Fujian Provincial Key Laboratory of Remote Sensing of Soil Erosion and Disaster Protection, China

ARTICLE INFO

ABSTRACT

Remote sensing is unique in its ability to record a variety of spatial and temporal data on land surfaces with complete coverage, especially at larger spatial scales, and it has been shown to be effective for rapidly recognizing spatio-temporal changes in regional eco-environments. This paper is the first to introduce a new remote sensing-based ecological index (RSEI) to assess the urban ecological quality. The RSEI integrated the primary land surface components (i.e., the build-up area and vegetation cover) and the climate (the land surface temperature and land surface moisture) based on the framework of the pressure-state-response (PSR) using a principal components analysis (PCA). In taking advantage of the same data source for all the indicators, the RSEI was shown to be scalable, visualizable and comparable at different spatio-temporal scales, and it can avoid the variation or error in weight definitions caused by individual characteristics. We used Fuzhou City in Fujian Province, south-eastern China, as a case study, it showed that Fuzhou demonstrated ecological improvements during the study period from 2000 to 2016, with its RSEI value increasing from 0.267 in 2000 to 0.503 in 2016. Moreover, the results of the spatial autocorrelation and semi-variance indicated that there was a spatial correlation in the distribution of the RSEI, with high clusters at the edge and low clusters in the centre of the city. The values of the sill, the nugget: sill ratio and the range all increased from 2000 to 2016, which indicated a higher spatial autocorrelation and lower spatial heterogeneity percentage in 2016 than that in 2000 in terms of the RSEI. Based on the combination with the spatial clusters and the spatiotemporal clusters, we confirmed that the RSEI is not randomly distributed. Moreover, a hole-effect semivariogram was observed, indicating a high level of human intervention in the study area. Specifically, the construction of the build-up area during the study period led to outward ecological degradation, and urban afforestation promoted environmental quality in the central urban area.

1. Introduction

China's economy has been growing rapidly since the early 1980s, in accordance with the government's reform policy, especially in the southeast coastal areas (http://gov.finance.sina.com.cn). This growth has accelerated the urbanization and industrialization in these regions, leading to dramatic land use and cover change (LUCC) from vegetation to built-up areas. Vegetative cover transformations are so pervasive that when aggregated in a certain place, they significantly impact the key aspects of local ecosystem functioning, such as biodiversity conservation, climate warming, urban heat islands, and water supplies (Xu et al., 2009; Hansen et al., 2013, Hu et al., 2016). Unfortunately, it is not simple to solve the environmental problems of today, but clearly, it is

necessary to monitor and assess the ecological state and changes to understand these complicated issues, and then conserve the ecological integrity (Dale and Beyeler, 2001; Lin et al., 2016). Fortunately, advances in the technologies of remote sensing (RS) and geographical information systems (GIS) have equipped ecologists with the tools to rapidly identify spatio-temporal changes in the environment (Kerr and Ostrovsky, 2003; Huang et al., 2012). However, despite the increasing effectiveness of remote sensing for use in large-scale environmental monitoring, the reliability of studies based on satellite data are still weakened by the uncertainty generated from human disturbances and spatial heterogeneity (Liu et al., 2006).

The pace, magnitude and spatial reach of human alterations of the earth's land surface are unprecedented (Lambin et al., 2001). Since

---

China initiated economic reforms and an open door policy in 1978, tremendous land-use changes have occurred in many coastal regions of China, such as the Yangtze River Delta region (Long et al., 2007), the Pearl River Delta region (Seto and Kaufmann, 2003) and the Golden Triangle Region (Xu et al., 2009). In these regions, accelerated industrialization and urbanization following economic reforms and population increases have greatly influenced land-use changes through increases in built-up areas and urban sprawl (Wu et al., 2004). For example, the conversion of cultivated land into non-agricultural land, such as construction land on the urban fringe or the countryside, has been considered a major feature of land-use change (Long et al., 2007). With the continuous growth of China's economy, environmental degradation induced by land use/cover change may occur without the appropriate planning and management of the existing land resources in these regions. Therefore, it is urgent to recognize the spatiotemporal dynamics of eco-environmental change in urban area where humans congregate, to provide scientific knowledge for the sustainable development of these regions.

In the early stage, plants were used as indicators to provide insights for assessing the physical processes and changes in environmental conditions (Clements, 1920), e.g., benthic and planktonic plants were used as indicator species to classify stream decomposition zones and estuarine and coastal eutrophication (Kolkwitz & Marsson, 1908; Paerl et al., 2003). In the past three decades, the use of ecological indicators has rapidly accelerated because of the universal need to evaluate ecological conditions for making protection or recovery decisions (Heinz Center, 2002; Honnay et al., 2003; Niemi and McDonald, 2004). Most of these ecological indices are based on an aggregation of selected sites to infer regional trends (Urquhart et al., 1998; Olsen et al., 1999), which are unsuitable for direct applications in a larger region (Urquhart et al., 1998; Kumar et al., 2017), and they cannot predict the global consequences of human activities (Zhang et al., 2016). In comparison with site-specific data, RS is unique in its ability to record a variety of spatial and temporal data over land surfaces with complete coverage, especially with regard to larger spatial scales, and it has been effective within a variety of applications (Groom et al., 2005; Zhang et al., 2016). However, these applications have usually focused on one aspect of the ecological status with a single ecological factor, such as the Normalized Difference Vegetation Index (NDVI) (Zhang et al., 2016) or the land surface temperature (LST) (Buyantuyev and Wu, 2010; Li et al., 2011). With the complexity of the system, e.g., greater spatio-temporal scales and increased human disturbance, it would be best to undertake a comprehensive consideration of various factors with a synthetic indicator (Suter et al., 2002). For instance, the United Nations conference on sustainable development (UNCSD) provided a theme-based framework that can explicitly assess the relationships between indicators and policies and highlight management targets (Bowen and Riley, 2003). De Keersmaecker et al. (2015) provided a framework to evaluate ecosystem stability for the major global RS ecosystems base.

Spatial heterogeneity refers to the uneven distribution of various concentrations of each observation (i.e., the species, terrain formation, and environmental characteristics) within a spatial domain (Herold et al., 2002; Wu, 2004). A landscape that shows spatial heterogeneity is one in which various patterns of land cover types are unevenly distributed across a region; they are nearly synonymous with "patchily distributed" (Herold et al., 2005; Liu et al., 2006), which can be indicated by remotely sensed pixel-wise values that are changed even in the instantaneous field of view (e.g., 1-km). This pattern is rooted in spatial heterogeneity, which in turn is grounded in variations in spatial dependence (Wu, 2004). Spatial dependence arises when the value of a pixel that is recorded at a location is highly related to the values at its surrounding locations (Wulder and Boots, 1998). These complicated issues in the imagery make it difficult to interpret and assimilate. Increasing numbers of recent studies have attempted to address the heterogeneity and homogeneity (i.e., spatial dependence) of remote-sensing-derived land surface parameters (Liu et al., 2006), e.g., the

normalized difference vegetation index (NDVI) (Wang et al., 2016), land surface temperature (LST) (Liu et al., 2006; Estoque et al., 2017), soil moisture (Qi et al., 2004), leaf area index (LAI) (Garrigues et al., 2006), and net primary production (NPP) (Sakai and Akiyama, 2005).

A number of techniques have been developed to assess the spatial variations in remotely sensed imagery. Because a landscape is regularized into a grid of equally sized and regularly spaced pixels, there must be a certain degree of dependency between pixels (Wulder and Boots, 1998). Early studies on this question have borrowed some indices from other disciplines, such as the Gini coefficient, the Ellison-Glaeser index and the Herfindahl index, to measure the spatial dependency (Bertinelli and Decrop, 2005; Goschin et al., 2009; Liu, 2014). Other global measures, such as Moran's I and Geary's C, are also widely used in empirical analyses (Carroll et al., 2008; Yang and Wong, 2013). However, these indices reflect the spatial correlations from a general perspective by incorporating all the samples, but they are unable to reveal whether those homogeneous pixels are in proximity to each other or if they are dispersed over the image (Wulder and Boots, 1998; Liu, 2014). One alternative to solving this problem is to use local indicators of spatial association (LISA) (Anselin, 1995). LISA measures the local spatial association and indicates the discrete spatial regimes (i.e., hot spots and cold spots) (Yang and Wong, 2013); thus, they have the potential to overcome the problems mentioned above. At present, besides the method of exploratory spatial data analysis (ESDA), semivariance analysis is also considered to be another extremely effective way to observe spatial characteristics (Zawadzki et al., 2009; Zawadzki and Fabijańczyk, 2013). Semivariance measures have traditionally been used to quantify the range of variability exhibited in the natural pattern of resource distributions (He et al., 2007; Hu et al., 2015). Additionally, it is worth mentioning here that the spatial heterogeneity in the observations may be affected by the arbitrariness in the definition of the scale (Wu, 2004), including the grain size (or resolution), extent and lag (or spacing) (Dungan et al., 2002). In this paper, it refers only to the "grain size".

The estuary lowland region of the Minjiang River in Fujian Province, south-eastern China, is composed of one primary coastal city, Fuzhou (Fig. 1). This city is one of the areas with the fastest economic growth in the country. Along with the development of the economy, the urban areas of the city have expanded rapidly in the past two decades, resulting in degraded habitability. Although this problem is poorly measured, it is critical for the urban planners and decision makers of this region. Therefore, a new remote sensing-based ecological index (RSEI) (Xu et al., 2013) was employed to assess the spatial-temporal variation in the ecological changes of Fuzhou City over the past 16 years using LISA and semivariance analysis techniques. This study aims to 1) monitor the long-term dynamics of the RSEI in this rapidly developing region from 2000 to 2016; 2) determine which grain size is the most suitable to analyse the spatial heterogeneity; 3) identify both static spatial clusters and temporal dynamic change clusters of RSEI; and 4) observe the characteristics (i.e., the nugget effect, sill, ranges and orientation effect) of spatial heterogeneity in the RSEI.

2. Methods and materials

2.1. Study area

Fuzhou City is the capital and the largest prefecture-level city in the Fujian Province of China (Fig. 1). It is situated in the west coast of the Taiwan Strait and in the lower reaches of the Minjiang River, which is the largest river within the province. The northern subtropical monsoon climate is prevailing in this area, with an average annual temperature of approximately 293.9 K. Annual precipitation varies widely from 796.5 to 1913.6 mm, of which approximately 33% is received in the May and June. The average elevation is 84 m, ranging from 1 m to 802 m. The study area (i.e., the red areas in Fig. 1b) locates in the central of the city, which is also the political and economic center of the city and even
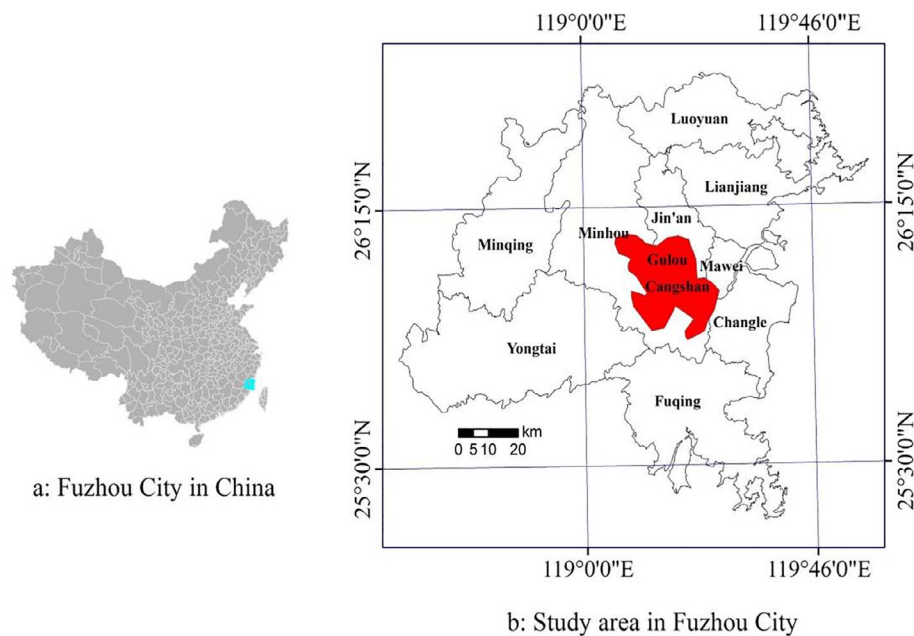
Fig. 1. Location of the study area.

of the Province, with construction and population being highly concentrated here. It has been reported that the quality of the ecosystem have declined dramatically during the past twenty years, characterizing with the notably warming climate in this area (Hu et al., 2015; Cai et al., 2016). Consequently, the study on the spatio-temporal pattern in the ecological quality of the area is meaningful, and can shed a light on those of rapidly growing cities in the world.

2.2. Data resources and pre-processing

During this study, Landsat images were acquired on 2000-05-04 (ETM+) and 2016-06-25 (OLI/TIRS) from USGS (https://glovis.usgs.gov/), over a period of 16 years. The images were in Level 1B, and they were systematically processed to provide geometric corrections prior to the analyses. First, the ETM + images were co-registered to the OLI/TIRS using nearest-neighbour re-sampling and a second-order polynomial with a mean RMSE of less than 0.5 pixels. Clouds and their shadows have been masked based on very low temperatures (Malbéteau et al., 2017). Additionally, the water patches have been masked based on the modified normalized difference water index (MNDWI) (Xu, 2006).

During the pre-processing of the datasets, the digit number (DN) values of the multispectral bands should be further converted into planetary surface reflectance values (Xu et al., 2013; Kilic et al., 2016). For Landsat ETM + imagery, the formula for the conversion of the at-aperture spectral radiance of the multispectral bands to planetary reflectance was expressed as indicated in the published literature (Chander et al., 2009). For Landsat OLI imagery, the processing of the calibration and the conversion to planetary surface reflectance was performed under the guidance of the Lansat-8 algorithm posted by the USGS (USGS, 2016a; http://glovis.usgs.gov/CDR_LSR.php).

To investigate the scale effects of the landscapes, the images were resampled into different grain sizes, including 30·30, 60·60, 90·90, 150·150, 300·300, 900·900, 1200·1200, 1500·1500 and 1800·1800 m^2.

2.3. Calculation of the remote sensing-based ecological index

In this case study, the RSEI is composed of a couple of indicators that can be quickly obtained from Landsat datasets at the pixel level. In this study, we employed the pressure-state-response (PSR) framework to define the RSEI. The PSR framework is based on the notion of causality (Hughey et al., 2004), which is built upon the selection and measurement of indicators for three categories, i.e., indicators of anthropogenic pressures, environmental states and climate responses. The indicators in the RSEI follow the general recommendations in the academic literature (Niemi and McDonald, 2004; Lin et al., 2016; Seddon et al., 2016). First, there is a general awareness that the ecological patterns and processes in certain regions are affected greatly by the activity of LUCC within their boundaries and beyond (Foley et al., 2005). Among them, the most notable physical feature is the change from ecological lands to construction purposes. Therefore, the normalized differential build-up and bare soil index (NDBSI) was applied to represent the intensity of the pressures on the environment originating from human activities. Second, indicators of environmental states are designed to describe the status quo of the environment and the quality and quantity of resources, and their changes over time; thus, NDVI, one of the most successful of many attempts to simply and quickly identify vegetated areas (Sun et al., 2010; Seddon et al., 2016), was selected as an indicator of the environmental state, describing the status quo of the environment and the quality and quantity of resources. Lastly, the LST and land surface moisture (LSM) were applied to indicate the local climate (i.e., temperature and humidity) changes in response to environmental changes and concerns. In taking advantage of the same data source for all the indicators, the RSEI has scalability, visualization and comparability at different spatio-temporal scales for different regions.

2.3.1. Normalized differential build-up and bare soil index

The index-based built-up index (IBI) has been commonly used to map built-up lands accurately (Xu, 2008; Essa et al., 2012). In addition to the built-up lands, patches of bare land or sparsely vegetated ground occurred in the deforested or abandoned locations across the study area. For this reason, a soil index (SI) was also employed to represent these bare areas. A combining index, NDBSI [Eq. (1)], which was composed of IBI [Eq. (2)] and SI [Eq. (3)], was proposed here.

$$NDBSI = (IBI + SI)/2 \tag{1}$$

$$\text{IBI} = \{2\rho_{SWI1}/(\rho_{SWI1} + \rho_{NIR}) - (\rho_{NIR}/(\rho_{NIR} + \rho_{Red}) + \rho_{Green}/(\rho_{Green} + \rho_{SWI1})]$$
$$/2\rho_{SWI1}/(\rho_{SWI1} + \rho_{NIR}) + [\rho_{NIR}/(\rho_{NIR} + \rho_{Red}) + \rho_{Green}/(\rho_{Green}$$
$$+ \rho_{SWI1})]\} \tag{2}$$

$$\text{SI} = [(\rho_{SWI1} + \rho_{Red}) - (\rho_{NIR} + \rho_{Blue})]/[(\rho_{SWI1} + \rho_{Red}) + (\rho_{NIR} + \rho_{Blue})] \tag{3}$$

where the ρ_i is the planetary reflectance of each band in the ETM + and OLI sensors, respectively; it is the same as indicated below.

2.3.2. Normalized differential vegetation index

The NDVI has been successfully utilized to monitor and assess vegetation cover across different scales (Xu and Zhang, 2013; Seddon et al., 2016). With the normalization of the spectral bands, the NDVI may reduce the effect of sensor degradation (Zheng et al., 2015). Most research suggests that the NDVI is sensitive to low density vegetation, and it is especially suitable for urban areas with high densities of built-up land (Wang et al., 2015; Liu et al., 2017). Thus, NDVI is employed here, and it is expressed in Eq. (4) as follows:

$$\text{NDVI} = (\rho_{NIR} - \rho_{Red})/(\rho_{NIR} + \rho_{Red}) \tag{4}$$

2.3.3. Land surface moisture

Due to the direct effect of the Tasseled Cap's components, such as the brightness, greenness and wetness on the physical parameters of the earth's surface (Zawadzki et al., 2016), the Tasseled Cap transformation has been extensively used in ecological monitoring studies (Crist, 1985; Goward et al., 2002; Huang et al., 2002). The wetness component is used as the LSM indicator here, as expressed in Eq. (5) as follows:

$$\text{LSM} = 0.0315\rho_{Blue} + 0.2021\rho_{Green} + 0.3102\rho_{Red} + 0.1594\rho_{NIR} - 0.6806\rho_{SWIR1}$$
$$- 0.6109\rho_{SWIR2} \tag{5}$$

2.3.4. Land surface temperature

The standard method for retrieving LST from raw Landsat datasets requires the conversion of the DN values of the thermal bands (Band 6 in Landsat ETM+, and Bands 10 and 11 in Landsat TIRS) into at-satellite spectral radiance values (L_λ) (Chander et al., 2009; Xu et al., 2009; USGS, 2016b) and then into the at-satellite brightness temperature (T_b), which is calculated under an assumption of unity emissivity (ε) and using pre-launch calibration constants (Chander et al., 2009; Xu et al., 2009; USGS, 2016b). This process is followed by a correction for spectral emissivity according to the nature of the landscape (Sobrino et al., 2004; Weng, 2009; Xu et al., 2013). In this study, we used the thermal Band 6 of Landsat ETM + and Band 10 of Landsat OLI to retrieve the LST for the years 2000 and 2016, respectively. The calculations of L_λ, T_b, ε and LST were performed in light of these references (Xu et al., 2009; Estoque et al., 2017).

2.3.5. Synthetic index of RSEI

Based on the above calculation of each factor in the PSR framework, we aimed to design the synthetic index (i.e., RSEI) that will allow for a quick and quantitative assessment of a region's ecological quality. The weighting method is among the most important processes in the building of the RSEI. Currently, there are many alternative weighting methods, e.g., AHP and Delphi (Cinelli et al., 2014; Norouzian-Maleki et al., 2015). However, even for this simple weighting method, the subjective experience may affect the weight distribution in practice. For this reason, a principal components analysis (PCA) was adopted to identify the relative importance of each variable. The PCA method is a multi-dimensional data compression technology that can remove any impact of co-linearity between the four variables (Seddon et al., 2016). More importantly, the weight of each factor is automatically and objectively allocated according to the contribution of each factor to the principal components, which can prevent the variation or error in the

weight definition caused by individual characteristics (Xu, 2013).

Before processing the PCA, all the factors (i.e., NDBSI, NDVI, LST and LSM) were rescaled between 0 and 1 (Carlson and Arthur, 2000; Xu et al., 2009). The PCA was then calculated in ENVI (version 5.1) software using the PCA Rotation tool; as a result, a single-band image (i.e., RSEI image) was created. During both study years, the percent eigenvalues of PC1 were both higher than 98% (98.41% for 2000 and 98.72% for 2016), indicating that this component has integrated most of the characteristics of all the variables, and thus PC1 was used to build the RSEI in this study. To facilitate the temporal comparison between the different study periods, the resulting RSEI values were again normalized from 0 to 1, with higher values indicating better ecological quality and lower values indicating poorer ecological quality.

2.4. Spatial heterogeneity analysis

2.4.1. Spatial autocorrelation analysis

ESDA is a set of techniques used to detect the spatial regimes for the observation (Anselin, 1999; Hu et al., 2015), and it can visualize the spatial agglomeration and anomalies of the RSEI (McMillen, 2010). It was applied to examine if the spatial autocorrelation of RSEI was present in Fuzhou City. The analysis focused on two aspects of spatial clustering, namely the overall "global" spatial clustering and the "local" patterns of RSEI distribution.

The global measure of Moran's I_g is as follows [Eq. (6)]:

$$I_g = \frac{N \sum_i \sum_j w_{ij}(x_i - \mu)(x_j - \mu)}{\left(\sum_i \sum_j w_{ij}\right) \sum_i (x_i - \mu)^2} \tag{6}$$

where w_{ij} is the row-standardized contiguity matrix and x_i and x_j are the RSEI at grids i and j, respectively, and μ is the average level of RSEI. N is the total number of the grids in the study area. Moran's I_g ranges from approximately + 1 (for positive spatial autocorrelation) to -1 (negative autocorrelation), and zero expresses the absence of spatial autocorrelation (Anselin, 2003).

The Moran's I_g cannot indicate hot spots and cold spots across the study area. Therefore, the local indicator of spatial association (LISA) was applied to measure the local spatial association and to indicate the significance of hot spots and cold spots (Hu et al., 2015). The local Moran's I_l statistic [Eq. (7)] was employed to show the LISA in this research.

$$I_l = \frac{x_i - \mu}{\sum_i (x_i - \mu)^2} \sum_j w_{ij}(x_j - \mu) \tag{7}$$

Both the globe Moran's I_g and the local Moran's I_l were calculated using the GeoDa program in this study (Anselin, 2003). When the program was run, the rook contiguity weighting method was adopted. The number of permutation tests was set to 999 and the significance level was set to 0.05. Then, a spatial typology map consisting of five categories of clusters in the RSEI was created, namely High-High (hotspots), Low-Low (cold-spots), Low–High, High-Low and "not significant" (Figs. 6 and 7, right).

2.4.2. Semivariance analysis

Additionally, we also employed semivariance, a central tool of geostatistics (Krige, 1966; Zawadzki et al., 2005; Chen and Feng, 2013), to measure the spatial continuity of the neighbouring RSEIs. The value of the experimental semivariance for a vector is derived from calculating one-half the average squared difference between every data pair separated by a specific lag distance of h (Krige, 1966; Hu et al., 2015). The standard equation for the semivariance is indicated in Eq. (8) as follows:

$$\gamma(h) = \frac{1}{2N(h)} \sum_{i=1}^{N(h)} [z(x_i) - z(x_i + h)]^2 \tag{8}$$

where $\gamma(h)$ is the experimental semivariance value at distance interval h describing the degree of autocorrelation that is present; $z(x_i)$ is the measured sample value (i.e., RSEI) at grid x_i; $z(x_i + h)$ is the sample value (i.e., RSEI) at grid $x_i + h$; and $N(h)$ is the total number of sample data pairs separated by distance h.

The following parameters are usually applied to identify the semivariance functions (Treitz and Howarth, 2000; Zawadzki et al., 2005; Hu et al., 2015): sill $(C_0 + C)$, range (A_0), nugget effect (C_0), spatially dependent structural variance (C), and the ratio of the Nugget effect (C_0) to the Sill $(C_0 + C)$. In this case, the experimental semivariance (either the isotropic or the anisotropic one) was fitted by linear, spherical, exponential and Gaussian models using GS^+ v 7.0 (GDS, 2004). The coefficient of determination (R^2) and the residual sum of squares (RSS) were used to compare the goodness of the semivariance models (i.e., linear, spherical, exponential and Gaussian models) (Davis and Sampson, 2002).

3. Results and discussions

3.1. Exploratory data analysis

The descriptive statistics of the RSEI indicated that the average RSEI value increased from 0.267 in 2000 to 0.503 in 2016; the medium value of RSEI also increased from 0.307 in 2000 to 0.480 in 2016 (Table 1). The negative skew in 2000 indicated that the tail on the left side of the probability density function was longer or fatter than the right side; conversely, the positive skew in 2016 indicated that the tail on the right side was longer or fatter than the left side. Overall, our case indicated that the eco-environmental quality of the study area was improved from 2000 to 2016. However, the previous study (Xu et al., 2013) in this area indicated that the eco-environmental quality was degraded during the period from 2001 to 2009. The opposite results may be due to the differences in the time and space scale. Our study covered the period from 2000 to 2016, while the previous study covered the period from 2001 to 2009; moreover, the study area of our study was larger than that of the previous one because the new development in the southern section of the study region in recent years was also involved in our study. This finding indicated that there is a scale effect (in both the duration and spatial range) in the distribution of RSEI.

Fig. 2 revealed the spatial distribution of RSEI in 2000 and 2016. In Fig. 2, the study area was divided into five categories according to the RSEI values using equal intervals, namely, excellent, good, moderate, fair and poor. In general, the eco-environment was poorer in the central section than it was in the peripheral areas close to the rural zone, with the red and yellow polygons concentrated in the central region and dark green in the border. A notable characteristic of the distribution in RSEI was that the environmentally poor areas were gathered in the centre in 2000, while it was more dispersed in 2016. The figures indicated that the ecosystem was improved in the old districts (i.e., the north-central areas of the study area) during the period from 2000 to 2016, while the ecosystem was degraded in the new districts, especially in the island of the study area. The improved polygons that occurred in the north-central areas benefited from the afforestation program implemented in the region, with many traditional industrial polluters within the urban centre being closed or moved to the suburbs (Hu et al., 2015). Undoubtedly yet simultaneously, the urban sprawl led to continuous environment deterioration from 2000 to 2016 (Cai et al., 2016). This finding verifies the previous finding, which indicated that the

urbanization and industrialization intensified the ecological land losses, leading to environmental degradation (Deng et al., 2008; Hu et al., 2015). Therefore, the smart growth and compact cities of North American and European countries should be introduced for the sustainable development of human-dominant ecosystems in China (Couch and Karecha 2006; Chen et al., 2008).

3.2. Scale effect of spatial heterogeneity

Spatial heterogeneity is prevalent on all different scales, and it constitutes the basis of the structure and function of landscapes, whether they are natural or artificial (Wu, 2004). To explain the spatiotemporal change mechanism in landscape structure and function as driven by biophysical and socioeconomic factors, the scale effect must be quantified (Dungan et al., 2002). Our results showed that there was spatial autocorrelation in the RSEI at all the grain size levels, with statistical significances that were all lower than 5%. This finding confirms the "first law in geography", which shows that "Everything is related to everything else, but near things are more related than distant things" (Tobler, 1970).

Fig. 3 indicated that the values of Moran's I and R^2 in the spatial autocorrelation analysis monotonically decreased with the increase in the grain size, with a sharper decline from $150\cdot150\ m^2$ in both of the study years. Figs. 4 and 5 indicated that the change in the A_0 values was large in the grain sizes of $30\cdot30\ m^2$, $60\cdot60\ m^2$ and $90\cdot90\ m^2$ in both of the years; however, from $150\cdot150\ m^2$, the parameter trended towards relative invariableness. The other parameters, such as $C_0 + C$, $C_0/(C_0 + C)$ and the R^2 of semivariances showed a relatively invariable trend except for the C_0 parameter.

Our analytical results are consistent with "the second law in geography", which indicates that "Everything is related to everything else, but things observed at a coarse spatial resolution are more related than things observed at a finer resolution" (Arbia et al., 1996). This law revealed the truth that the variance in RSEI decreased with the increase in the grain size in this study.

The spatial heterogeneity may exhibit various paradigms at different scales (i.e., grain sizes), and this pattern can be best characterized at a certain scale (Lam and Quattrochi, 1992). Based on the analysis, $150\cdot150\ m^2$ was viewed as a suitable grain size to weaken the scale effects in this study. Thus, it was applied here during the observation of the spatial pattern of the RSEI distribution.

3.3. Spatial heterogeneity in RSEI

3.3.1. Spatial autocorrelation analysis

The value of Moran's I has a range from -1 to 1. A value greater than zero indicates a positive spatial autocorrelation; a value of less than zero shows a negative spatial autocorrelation (Li et al., 2017). The Moran's I_g of the RSEI at different spatial scales was indicated in Fig. 6. Overall, the curve showed a downward trend, indicating that the spatial variation in the RSEI increased with the increasing spatial distance. Over a range of 10 km or so, the spatial association of RSEI was positive while changing to negative beyond 10 km or so.

In this study, LISA was employed to detect both the spatial clusters and the spatiotemporal clusters of RSEI. The spatial clusters aimed to identify areas with high-high (hot-spot) or low-low (cold-spot) patterns throughout the entire study region during certain periods (Fig. 7), while the spatiotemporal clusters aimed to identify areas with changing dynamics (i.e., ones that were degraded or improved) during the study period (Fig. 8). In Fig. 7, High-High/Low-Low signifies that the statistically significant regions of good/poor quality were surrounded by their homogeneous regions, respectively; High-Low/Low-High indicates the statistically significant regions in good/poor quality surrounded by their heterogeneous regions, respectively. In Fig. 8, High-High/Low-Low indicates that the regions of statistically significantly improved/degraded regions were surrounded by areas with the same direction of

Table 1
Description statistics of RSEI.

	Min	Max	Average	S.D.	Skewness	Kurtosis	Medium
2000	−0.264	0.671	0.267	0.205	−1.002	3.449	0.307
2012	0.089	0.810	0.503	0.131	0.412	2.167	0.480
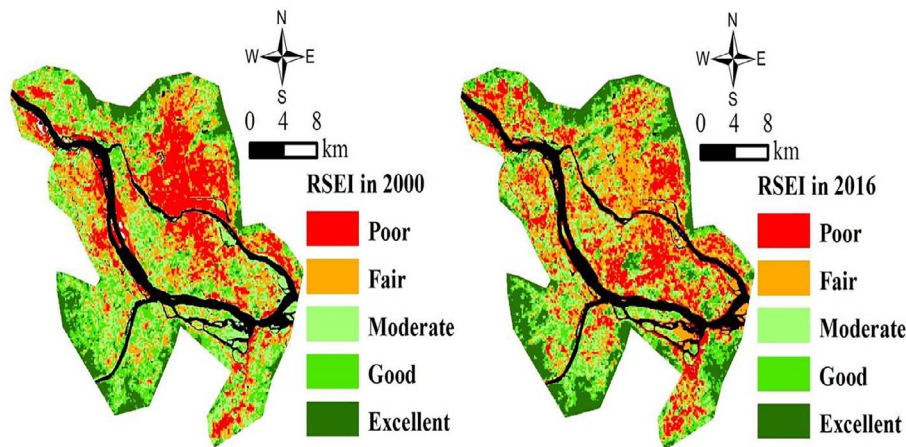
Fig. 2. Spatial distribution of RSEI in 2000 and 2016.
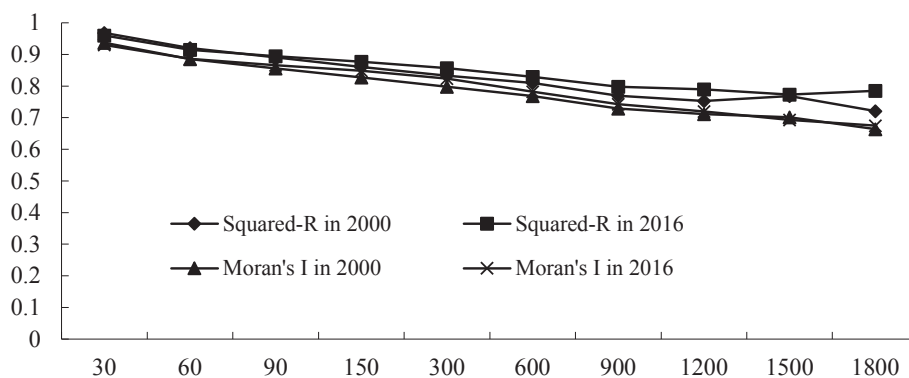
Fig. 3. Parameters of spatial autocorrelation respond to grain sizes in years of 2000 and 2016.

change in the RSEI as themselves during the study period. High-Low/Low-High indicates that the statistically significant improved/degraded regions were surrounded by areas with the opposite direction of change in the RSEI as themselves during the study period.

Fig. 7 shows that the High-High clusters were distributed around the study area in both study years. However, the Low-Low clusters were concentrated in the old downtown in 2000 while moving to the periphery of the previous clusters in 2016. Fig. 8 (left) also indicates that the eco-environmental quality in the old downtown was improved from 2000 to 2016. Fig. 8 (right) revealed that the statistically significant High-High/Low-Low clusters were all in the improved/degraded areas in Fig. 8 (left), respectively.

The clusters obtained from these two methods (i.e., both the spatial clusters and the spatiotemporal clusters mentioned above) led to similarly deteriorated clusters (i.e., the blue polygons in Figs. 7 and 8)

and improved clusters (i.e., the red polygons in Figs. 7 and 8). It is thus confirmed that the RSEI is not randomly distributed. Therefore, it is not difficult to judge that the extension of the built-up area during the study period led to the appearance of these Low-Low clusters in 2016, and urban afforestation promoted good environmental quality in the urban central area (Hu et al., 2015).

3.3.2. Semivariance analysis

Table 2 describes the parameters of the fitting models in the isotropic variogram for RSEI in the years 2000 and 2016. These models best satisfied the hypothesis according to the R^2 and RSS values (Zawadzki et al., 2005; Liu et al., 2013).

The nugget effect (C_0) represents spatially independent variability, including the measurement error and short-scale variations that occur at a scale smaller than the closest sampling interval (i.e., the pixel size)
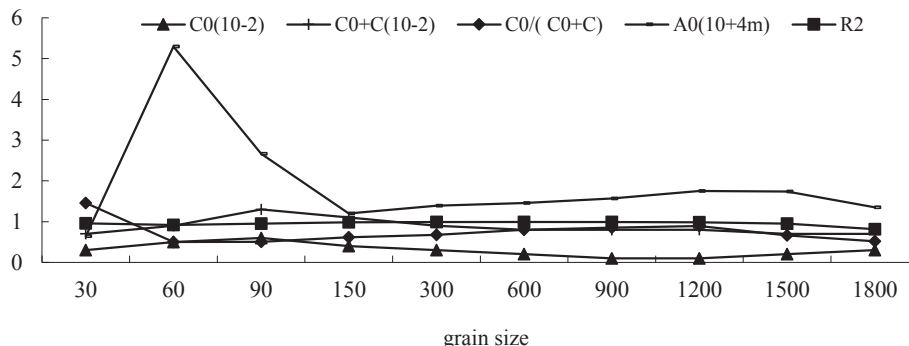
Fig. 4. Parameters of spatial heterogeneity respond to grain sizes in 2000.
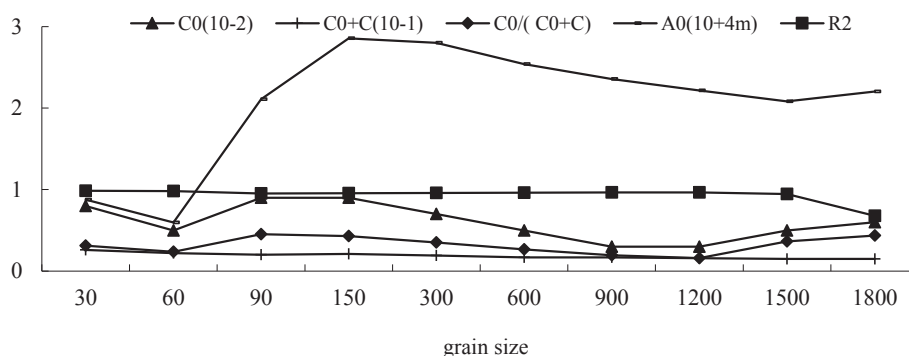
Fig. 5. Parameters of spatial heterogeneity respond to grain sizes in 2016.

(Huijbregts, 1975). According to the parameters, the values of the nugget effect (C_0) for the isotropic variograms were 0.004 in 2000 and 0.009 in 2016 (Table 2), indicating that the spatially independent variabilities generally arose from measurement errors (including sampling error) were small, and the measurements therein could be used to analyse the spatial variation of the RSEI in question.

The spatial variations increased with the increasing interval (lag-distance) (Figs. 9 and 10), and they reached a stable plateau, which is called the sill ($C_0 + C$). The sill is the sum of the total variation, including the nugget effect and the spatial inequality (Zawadzki et al., 2005). The nugget/sill ratio [$C_0/(C + C_0)$] reveals the spatial correlation degree of regional variables, with a ratio < 0.25 indicating strong spatial correlation, a ratio of 0.25–0.75 indicating moderate spatial correlation, and a ratio > 0.75 indicating weak spatial correlation (Cambardella et al., 1994; Javed et al., 2005). Table 2 shows that the values of the sill were 0.011 in 2000 and 0.021 in 2016; moreover, the values of the $C_0/(C + C_0)$ were 0.383 and 0.430 in 2000 and 2016, respectively. These parameters indicated that the structural factors were leading sections for spatial patterns and there was spatial dependence in the distribution of the RSEI, which is consistent with the result of the spatial autocorrelation analysis.

Their range (A_0) indicates the distance at which the spatial correlation of the pixel properties disappears and therefore presents a measurement of the size of the spatial variations embedded within the distribution of the RSEI expressed by the semivariance (Figs. 9 and 10). Beyond the distance, the spatial interpolation or processing is invalid (Yuan et al., 2015). In this case, the models revealed that the RSEI distributions were fully independent when the observing distance exceeded 12 km in 2000 and 29 km in 2016 (Table 2).

The values of the sill, the nugget/sill ratio and the range all increased from 2000 to 2016 (Table 2), which indicated that there was a higher spatial autocorrelation and lower spatial heterogeneity percentage in the RSEI in 2016 than in 2000. This trend implies that the urbanization process has a significant effect on the spatial structure of the eco-environment as measured by RSEI. The effect was a double-edged sword as discussed in Section 3.3.1. This finding shows that the results of these two methods (i.e., spatial autocorrelation analysis and

semivariance analysis) are consistent, and only the combination of these two methods can better explain the spatial paradigm of the observation.

The calculation of the experimental semivariance considering all the pixels in all directions within the entire study area is the most rigorous approach, but it is a very time-consuming process due to the large number of observations involved in the calculation (Balaguer-Beser et al., 2013). To overcome this weakness, a multidirectional approach (i.e., anisotropic semivariance), which is defined as the experimental semivariance, is obtained by computing a limited number of analysed directions (Maillard, 2003), which was also employed here. In this study, both the isotropic and the anisotropic semivariances were performed and compared. The anisotropic semivariances were calculated by taking the mean of each pixel in several transects (i.e., directions) over a range from 0° to 180°, in which four directions, the north-south direction (0°), northeast-southwest direction (45°), west-east direction (90°) and southeast-northwest direction (135°), were observed here. Figs. 9 and 10 show that the trend in the semivariance curves for both the isotropic and anisotropic models were similar. All the curves indicated that the semivariance values tend to be higher as the lag distance increases in general, but they are not monotonic. However, the semivariance showed a cyclical behaviour, which is known as the hole-effect semivariogram, which is characterized by having crest(s) and valley(s) in a curve (Pyrcz and Deutsch, 2003), and it is commonly found in areas with a high intensity of human intervention (Balaguer-Beser et al., 2013). This finding is consistent with this study that used an urban area as the observation object, in which populations and buildings were highly concentrated. According to the indices of the fractal dimension (D) for both the isotropic and anisotropic models (Table 3), the results of the variance analysis revealed that there was no significant difference in the distribution of RSEI among all the directions.

4. Conclusions

A new index known as RSEI, which was based on the PSR framework, was applied to evaluate the regional ecological status. It may help
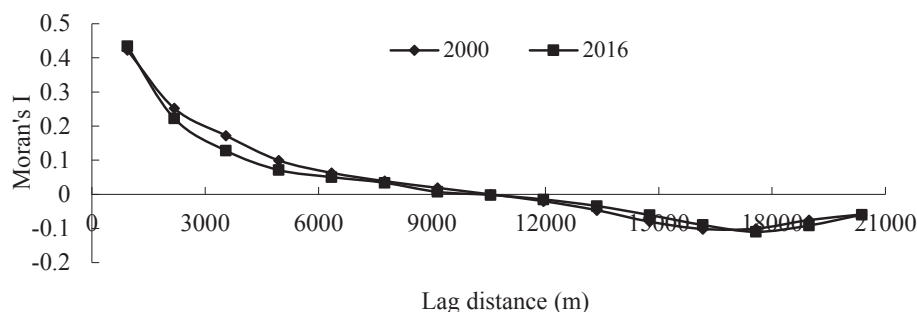
Fig. 6. Moran's I_g of RSEI responds to distances in 2000 and 2016.
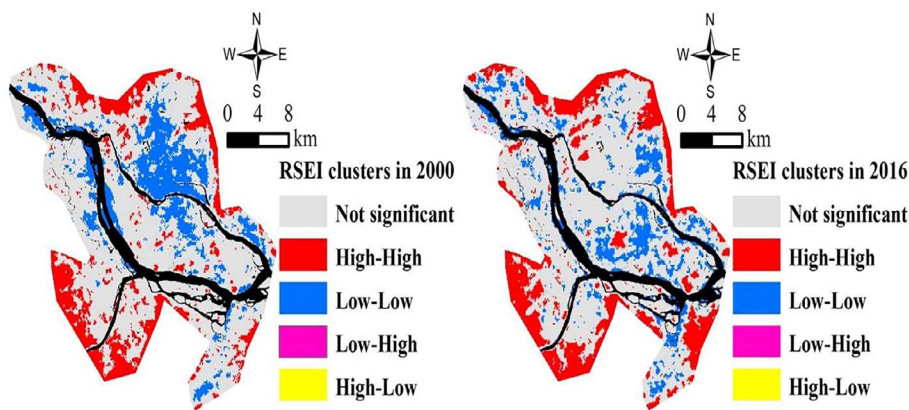
Fig. 7. Significant clusters of RSEI in 2000 and 2016.
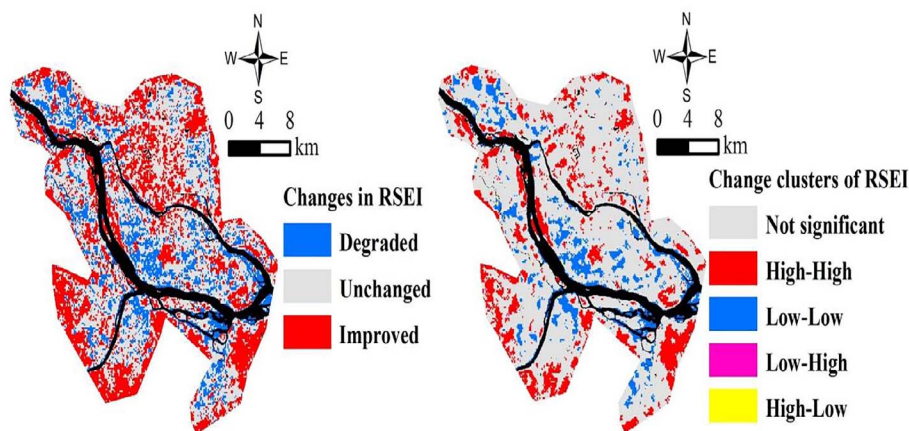
Fig. 8. Changes and their significant clusters of RSEI from 2000 to 2016.

Table 2
Parameters of spatial heterogeneity of RSEI in 2000 and 2016 (150 m).

	C_0	C	$C_0 + C$	$C_0/(C_0 + C)$	A_0 (m)	R^2	RSS
2000	0.004	0.007	0.011	0.383	12,030	0.985	$5.385E - 07$
2016	0.009	0.012	0.021	0.430	28,560	0.956	$5.493E - 06$

us understand the variation in the pressure, state and response of the ecosystem. RSEI was formed using the PC1 derived from the four factors and thus it can measure the pressures on the environment caused by human activities (i.e., urbanization), changes in the environmental state (i.e., vegetation coverage) and the climate change responses (i.e., temperature and humidity). In using the advantage of having the same data source for all the indicators, the RSEI was found to be scalable, visualizable and comparable at different spatio-temporal scales and can avoid the variation or error in weight definitions caused by individual characteristics. In using Fuzhou City of Fujian Province in south-eastern China as a case, the results showed that Fuzhou experienced ecological improvements during the study period from 2000 to 2016, with the RSEI value increasing from 0.267 in 2000 to 0.503 in 2016.

A set of parameters was then extracted from the autocorrelation and semivariance analysis (both of which are omnidirectional and multi-directional) to quantify the heterogeneity of the spatial distribution in the RSEI. Based on the analysis, $150 \cdot 150 \, m^2$ was viewed as a suitable grain size to weaken the scale effects in this study. The analysis of the spatial autocorrelation and semivariance indicated that there was spatial correlation in the distribution of the RSEI, with the high value in the edge and the low value in the centre of the city. The values of the sill, the nugget/sill ratio and the range all increased from 2000 to 2016. Based on the combination with the spatial clusters and the spatio-temporal clusters, we confirmed that the RSEI is not randomly
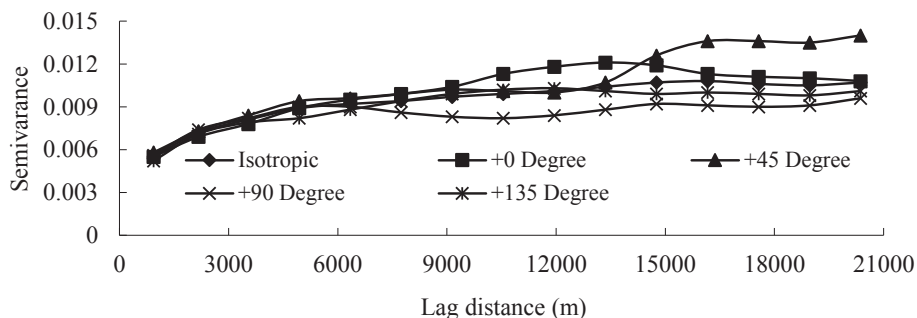
Fig. 9. Parameters of spatial heterogeneity of RSEI for different directions in 2000 (150 m).
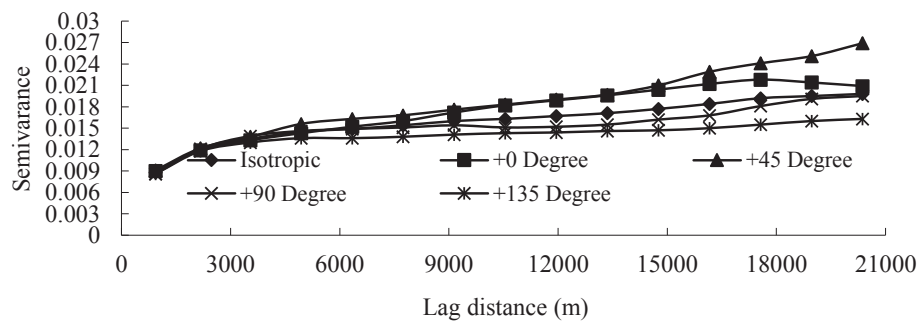
Fig. 10. Parameters of spatial heterogeneity of RSEI for different directions in 2016 (150 m).

Table 3
Fractal dimension of spatial heterogeneity in RSEI for different directions in 2000 and 2016 (150 m).

	Isotropic			+0°			+45°			+90°			+135°		
	D	SE	R^2	D	SE	R^2	D	SE	R^2	D	SE	R^2	D	SE	R^2
2000	1.897	0.104	0.963	1.877	0.158	0.916	1.863	0.142	0.930	1.936	0.317	0.741	1.901	0.174	0.902
2016	1.881	0.077	0.979	1.856	0.051	0.990	1.839	0.098	0.965	1.894	0.176	0.899	1.917	0.173	0.905

distributed. Moreover, a hole-effect semivariogram was observed, indicating a high level of human intervention in the study area. Specifically, the construction of the built-up area during the study period led to ecological degradation outward, and urban afforestation promoted good environmental quality in the central urban area. In this case, we suggested that the observations were fully independent when the observation distance exceeded 12 km in 2000 and 29 km in 2016. Hence, this research sheds light on the applications of ESDA and semivariance analysis to assess urban eco-environment changes using the remote sensing index.

Acknowledgements

References

Anselin, L., 2003. GeoDa 0.9 User's Guide. Spatial Analysis Laboratory (SAL). Department of Agricultural and Consumer Economics, University of Illinois, Urbana-Champaign, IL.

Anselin, L., 1999. Interactive techniques and exploratory spatial data analysis. In: Longley, P.A., Godchild, M.F., Maguire, D.J. (Eds.), Geographical Information Systems. John Wiley & Sons, New York.

Anselin, L., 1995. Local indicators of spatial association-LISA. Geograph. Anal. 27, 93–115.

Arbia, G., Benedetti, R., Espa, G., 1996. Effects of the MAUP on image classification. Geograph. Syst. 3, 123–141.

Balaguer-Beser, A., Ruiz, L.A., Hermosilla, T., Recio, J.A., 2013. Using semivariogram indices to analyse heterogeneity in spatial patterns in remotely sensed images. Comput. Geosci. 50, 115–127.

Bertinelli, L., Decrop, J., 2005. Geographical agglomeration: Ellison and Glaeser's index applied to the case of Belgian manufacturing industry. Reg. Stud. 39, 567–583.

Bowen, R.E., Riley, C., 2003. Socio-economic indicators and integrated coastal management. Ocean Coast. Manage. 46, 299–312.

Buyantuyev, A., Wu, J., 2010. Urban heat islands and landscape heterogeneity: linking spatiotemporal variations in surface temperatures to land-cover and socioeconomic patterns. Landscape Ecol. 25, 17–33.

Cai, Y.B., Zhang, H., Zheng, P., Pan, W.B., 2016. Quantifying the impact of land use/land cover changes on the urban heat island: a case study of the natural wetlands distribution area of Fuzhou City, China. Wetlands 36, 285–298.

Cambardella, C.A., Moorman, T.B., Parkin, T.B., Karlen, D.L., Turco, R.F., Konopka, A.E., 1994. Field scale variability of soil properties in central Iowa soils. Soil Sci. Soc. Am. J. 58, 1501–1511.

Carlson, T.N., Arthur, S.T., 2000. The impact of land use-land cover changes due to urbanization on surface microclimate and hydrology: a satellite perspective. Global

Planet. Change 25, 49–65.

Carroll, M.C., Reid, N., Smith, B.W., 2008. Location quotients versus spatial autocorrelation in identifying potential cluster regions. Ann. Reg. Sci. 42, 449–463.

Chander, G., Markham, B.L., Helder, D.L., 2009. Summary of current radiometric calibration coefficients for LandsatMSS, TM, ETM +, and EO-1 ALI sensors. Remote Sens. Environ. 113, 893–903.

Chen, H., Jia, B., Lau, S.S.Y., 2008. Sustainable urban form for Chinese compact cities: challenges of a rapid urbanized economy. Habitat Int. 32, 28–40.

Chen, L.J., Feng, Q., 2013. Geostatistical analysis of temporal and spatial variations in groundwater levels and quality in the Minqin oasis, Northwest China. Environ. Earth Sci. 70, 1367–1378.

Cinelli, M., Coles, S.R., Kirwan, K., 2014. Analysis of the potentials of multi criteriadecision analysis methods to conduct sustainability assessment. Ecol. Ind. 46, 138–148.

Clements, F.C., 1920. Plant Indicators. Carnegie Inst, Washington, DC.

Couch, C., Karecha, J., 2006. Controlling urban sprawl: some experiences from Liverpool. Cities 23, 353–363.

Crist, E.P., 1985. A TM tasseled cap equivalent transformation for reflectance factor data. Remote Sens. Environ. 17, 301–306.

Dale, V.H., Beyeler, S.C., 2001. Challenges in the development and use of ecological indicators. Ecol. Ind. 1, 3–10.

Davis, J.C., Sampson, R.J., 2002. Statistics and data analysis in geology, third ed. John Wiley & Sons, New York.

De Keersmaecker, W., Lhermitte, S., Tits, L., Honnay, O., Somers, B., Coppin, P., 2015. Resilience and the reliability of spectral entropy to assess ecosystem stability. Glob. Change Biol. 145, 39–44.

Deng, X.Z., Huang, J.K., Rozelle, S., Uchida, E., 2008. Growth, population and industrialization, and urban land expansion of China. J. Urban Econ. 63, 96–115.

Dungan, J.L., Perry, J.N., Dale, M.R.T., Legendre, P., Citron-Pousty, S., Fortin, M.J., Jakomulska, A., Miriti, M., Rosenberg, M.S., 2002. A balanced view of scale in spatial statistical analysis. Ecography 25, 626–640.

Essa, W., Verbeiren, B., van der Kwast, J., Van de Voorde, T., Batelaan, O., 2012. Evaluation of the DisTrad thermal sharpening methodology for urban areas. Int. J. Appl. Earth Obs. Geoinf. 19, 163–172.

Estoque, R.C., Murayama, Y., Myint, S.W., 2017. Effects of landscape composition and pattern on land surface temperature: an urban heat island study in the megacities of Southeast Asia. Sci. Total Environ. 577, 349–359.

Foley, J.A., De Fries, R., Asner, G.P., Barford, C., Bonan, G., Carpenter, S.R., Chapin, F.S., Coe, M.T., Daily, G.C., Gibbs, H.K., Helkowski, J.H., Holloway, T., Howard, E.A., Kucharik, C.J., Monfreda, C., Patz, J.A., Prentice, I.C., Ramankutty, N., Snyder, P.K., 2005. Global consequences of land use. Science 309, 570–574.

Gamma Design Software (GDS), 2004. GS +: Geostatistics for the Environmental Sciences. Gamma Design Software, Plainwell, Michigan USA.

Garrigues, S., Allard, D., Baret, F., Weiss, M., 2006. Influence of landscape spatial heterogeneity on the non-linear estimation of leaf area index from moderate spatial resolution remote sensing data. Remote Sens. Environ. 105, 286–298.

Goschin, Z., Constantin, D.L., Roman, M., Ileanu, B., 2009. Regional specialization and geographical concentration of industries in Romania. South-Eastern Eur. J. Econ. 1, 99–113.

Goward, S.N., Xue, Y.K., Czajkowski, K.P., 2002. Evaluating land surface moisture conditions from the remotely sensed temperature/vegetation index measurements: an exploration with the simplified simple biosphere model. Remote Sens. Environ. 79, 225–242.

Groom, G., Mücher, C.A., Ihse, M., Wrbka, T., 2005. Remote sensing in landscape ecology: experiences and perspectives in a European context. Landscape Ecol. 20, 391–408.

Hansen, M.C., Potapov, P.V., Moore, R., Hancher, M., Turubanova, S.A., Tyukavina, A., Thau, D., Stehman, S.V., Goetz, S.J., Loveland, T.R., Kommareddy, A., Egorov, A., Chini, L., Justice, C.O., Townshend, J.R.G., 2013. High-resolution global maps of 21st-century forest cover change. Science 342, 850–853.

He, Z.B., Zhao, W.Z., Chang, X.L., 2007. The modifiable areal unit problem of spatial heterogeneity of plant community in the transitional zone between oasis and desert using semivariance analysis. Landscape Ecol. 22, 95–104.

Center, Heinz, 2002. The State of the Nation's Ecosystems: Measuring the Lands, Waters, and Living Resources of the United States. Cambridge Univ. Press, New York.

Herold, M., Couclelis, H., Clarke, K.C., 2005. The role of spatial metrics in the analysis and modeling of urban land use change. Comput. Environ. Urban Syst. 29, 369–399.

Herold, M., Scepan, J., Clarke, K.C., 2002. The use of remote sensing and landscape metrics to describe structures and changes in urban land uses. Environ. Plann. A 34, 1443–1458.

Honnay, O., Piessens, K., Van Landuyt, W., Hermy, M., Gulinck, H., 2003. Satellite based land use and landscape complexity indices as predictors for regional plant species diversity. Landscape Urban Plann. 63, 241–250.

Hu, X.S., Hong, W., Qiu, R.Z., Hong, T., Chen, C., Wu, C.Z., 2015. Geographic variations of ecosystem service intensity in Fuzhou City, China. Sci. Total Environ. 512–513, 215–226.

Hu, X.S., Wu, Z.L., Wu, C.Z., Ye, L.M., Lan, C.F., Tang, K., Xu, L., Qiu, R.Z., 2016. Effects of road network on diversiform forest cover changes in the highest coverage region in China: an analysis of sampling strategies. Sci. Total Environ. 565, 28–39.

Huang, C., Wylie, B., Yang, L., Homer, C., Zylstra, G., 2002. Derivation of a Tasselled Cap transformation based on Landsat 7 at-satellite reflectance. Int. J. Remote Sens. 23 (8), 1741–1748.

Huang, J.L., Pontius Jr, R.G., Li, Q.S., Zhang, Y.J., 2012. Use of intensity analysis to link patterns with processes of land change from 1986 to 2007 in a coastal watershed of southeast china. Appl. Geogr. 34, 371–384.

Hughey, K.F.D., Cullen, R., Kerr, G.N., Cook, A.J., 2004. Application of the pressure-state-response framework to perceptions reporting of the state of the New Zealand environment. J. Environ. Manage. 70, 85–93.

Huijbregts, C.J., 1975. Regionalized variables and quantitative analysis of spatial data. In: Davis, J.C., McCullagh, M.J. (Eds.), Display and Analysis of Spatial Data. John Wiley & Sons, London, pp. 38–53.

Javed, I., Thomasson, J.A., Jenkins, J.N., Owens, P.R., Whisler, F.D., 2005. Spatial variability analysis of soil physical properties of alluvial soils. Soil Sci. Soc. Am. J. 69, 1338–1350.

Kerr, J.T., Ostrovsky, M., 2003. From space to species: ecological applications for remote sensing. Trends Ecol. Evol. 18, 299–305.

Kilic, A., Allen, R., Trezza, R., Ratcliffe, I., Kamble, B., Robison, C., Ozturk, D., 2016. Sensitivity of evapotranspiration retrievals from the METRIC processing algorithm to improved radiometric resolution of Landsat 8 thermal data and to calibration bias in Landsat 7 and 8 surface temperature. Remote Sens. Environ. 185, 198–209.

Kolkwitz, R., Marsson, M., 1908. Oˆ kologie der pflanzlichen Saprobien. Bericht der Deutschen Botanischen Gesellschaft 26, 505–519.

Krige, D.G., 1966. A study of gold and uranium distribution patterns in the Klerksdorp gold field. Geoexploration 4, 43–53.

Kumar, P., Thakur, P.K., Bansod, B.K., Debnath, S.K., 2017. Multi-criteria evaluation of hydro-geological and anthropogenic parameters for the groundwater vulnerability assessment. Environ. Monit. Assess. 189, 564.

Lam, N.S.-N., Quattrochi, D.A., 1992. On the issues of scale, resolution, and fractal analysis in the mapping sciences. Prof. Geogr. 44, 88–98.

Lambin, E.F., Turner, B.L., Geist, H.J., Agbola, S.B., Angelsen, A., Bruce, J.W., Coomes, O.T., Dirzo, R., Fischer, G., Folke, C., George, P.S., Homewood, K., Imbernon, J., Leemans, R., Li, X., Moran, E.F., Mortimore, M., Ramakrishnan, P.S., Richards, J.F., Skanes, H., Steffen, W., Stone, G.D., Svedin, U., Veldkamp, T.A., Vogel, C., Xu, J.C., 2001. The causes of land-use and land-cover change: moving beyond the myths. Global Environ. Change 11, 261–269.

Li, J.X., Song, C.H., Cao, L., Zhu, F.G., Meng, X.L., Wu, J.G., 2011. Impacts of landscape structure on surface urban heat islands: a case study of Shanghai, China. Remote Sens. Environ. 115, 3249–3263.

Li, R.Z., Cheng, S.H., Luo, C., Rutherford, S., Cao, J., Xu, Q.Q., Liu, X.D., Liu, Y.X., Xue, F.Z., Xu, Q., Li, X.J., 2017. Epidemiological characteristics and spatial-temporal clusters of mumps in Shandong Province, China, 2005–2014. Sci. Rep. 7, 46328.

Lin, T., Ge, R.B., Huang, J., Zhao, Q.J., Lin, J.Y., Huang, N., Zhang, G.Q., Li, X.H., Ye, H., Yin, K., 2016. A quantitative method to assess the ecological indicator system's effectiveness: a case study of the ecological province construction indicators of China. Ecol. Ind. 62, 95–100.

Liu, Z.Q., 2014. Global and local: measuring geographical concentration of China's manufacturing industries. The Professional Geographer 66, 284–297.

Liu, Q., Xie, W.J., Xia, J.B., 2013. Using semivariogram and Moran's I techniques to evaluate spatial distribution of soil micronutrients. Commun. Soil Sci. Plant Anal. 44, 1182–1192.

Liu, R.G., Shang, R., Liu, Y., Lu, X.L., 2017. Global evaluation of gap-filling approaches for seasonal NDVI with considering vegetation growth trajectory, protection of key point, noise resistance and curve stability. Remote Sens. Environ. 189, 164–179.

Liu, Y.B., Hiyama, T., Yamaguchi, Y., 2006. Scaling of land surface temperature using satellite data: a case examination on ASTER and MODIS products over a heterogeneous terrain area. Remote Sens. Environ. 105, 115–128.

Long, H., Tang, G., Li, X., Heilig, G.K., 2007. Socio-economic driving forces of land-use change in Kunshan, the Yangtze River Delta economic area of china. J. Environ. Manage. 83, 351–364.

Maillard, P., 2003. Comparing texture analysis methods through classification. Photogramm. Eng. Remote Sens. 69, 357–367.

Malbéteau, Y., Merlin, O., Gascoin, S., Gastellu, J.P., Mattar, C., Olivera-Guerra, L.,

Khabba, S., Jarlan, L., 2017. Normalizing land surface temperature data for elevation and illumination in mountainous areas: a case study using aster data over a steep-sided valley in Morocco. Remote Sens. Environ. 25–39.

McMillen, D.P., 2010. Issues in spatial data analysis. J. Reg. Sci. 50, 119–141.

Niemi, G.J., McDonald, M.E., 2004. Application of ecological indicators. Annu. Rev. Ecol. Evol. Syst. 35, 89–111.

Norouzian-Maleki, S., Bell, S., Hosseini, S.B., Faizi, M., 2015. Developing and testing aframework for the assessment of neighbourhood liveability in two contrasting countries: Iran and Estonia. Ecol. Ind. 48, 263–271.

Olsen, A.R., Sedransk, J., Edwards, D., Gotway, C.A., Liggett, W., Rathbun, S., Reckhow, K.H., Yyoung, L.J., 1999. Statistical issues for monitoring ecological and natural resources in the United States. Environ. Monit. Assess. 54, 1–45.

Paerl, H.W., Valdes, L.M., Pinckney, J.L., Piehler, M.F., Dyble, J., Moisander, P.H., 2003. Phytoplankton photopigments as indicators of estuarine and coastal eutrophication. Bioscience 53, 953–964.

Pyrcz, M.J., Deutsch, C.V., 2003. The whole story on the hole effect. In: Searston, S. (Ed.), Geostatisitical Association of Australasia. Newsletter, pp. 18.

Qi, F., Liu, Y.S., Ikami, M., 2004. Geostatistical analysis of soil moisture variability in grassland. J. Arid Environ. 58, 357–372.

Sakai, T., Akiyama, T., 2005. Quantifying the spatio-temporal variability of net primary production of the understory species, Sasa senanensis, using multipoint measuring techniques. Agric. For. Meteorol. 134, 60–69.

Seddon, A.W.R., Macias-Fauria, M., Long, P.R., Benz, D., Willis, K.J., 2016. Sensitivity of global terrestrial ecosystems to climate variability. Nature 531 (7593).

Seto, K.C., Kaufmann, R.K., 2003. Modeling the drivers of urban land use change in the Pearl River Delta, China: integrating remote sensing with socio-economic data. Land Econ. 79, 106–121.

Sobrino, J.A., Jiménez-Muñoz, J.C., Paolini, L., 2004. Land surface temperature retrieval from LANDSAT TM 5. Remote Sens. Environ. 90, 434–440.

Sun, Z.D., Chang, N.B., Opp, C., 2010. Using SPOT-VGT NDVI as a successive ecological indicator for understanding the environmental implications in the Tarim River Basin, China. J. Appl. Remote Sens. 4, 844–862.

Suter, G.W., Norton, S.B., Cormier, S.M., 2002. A methodology for inferring the causes of observed impairments in aquatic ecosystems. Environ. Toxicol. Chem. 21, 1101–1111.

Tobler, W., 1970. A computer movie simulating urban growth in the Detroit region. Econ. Geogr. 46, 234–240.

Treitz, P., Howarth, P., 2000. High spatial resolution remote sensing data for forest ecosystem classification: an examination of spatial scale. Remote Sens. Environ. 72, 268–289.

United States Geological Survey (USGS), 2016a. Product Guide: Provisional Landsat 8 Surface Reflectance Product. Geological Survey, Department of the Interior, U.S.

United States Geological Survey (USGS), 2016b. Landsat 8 (L8) Data Users Handbook. Geological Survey, Department of the Interior, U.S.

Urquhart, N.S., Paulsen, S.G., Larsen, D.P., 1998. Monitoring for policy-relevant regional trends over time. Ecol. Appl. 8, 246–257.

Wang, H., Liu, D., Lin, H., Montenegro, A., Zhu, X., 2015. NDVI and vegetation phenology dynamics under the influence of sunshine duration on the Tibetan plateau. Int. J. Climatol. 47, 855–870.

==Wang, J.F., Zhang, T.L., Fu, B.J., 2016. A measure of spatial stratified heterogeneity. Ecol. Ind. 67, 250–256.==

Weng, Q., 2009. Thermal infrared remote sensing for urban climate and environmental studies: methods, applications, and trends. ISPRS J. Photogramm. Remote Sens. 64, 335–344.

Wu, J.G., 2004. Effects of changing scale on landscape pattern analysis: scaling relations. Landscape Ecol. 19, 125–138.

Wu, L.X., Sun, B., Zhou, S.L., Huang, S.E., Zhao, Q.G., 2004. A new fusion technique of remote sensing images for land use/cover. Pedosphere 14, 187–194.

Wulder, M., Boots, B., 1998. Local spatial autocorrelation characteristics of remotely sensed imagery assessed with the Getis statistic. Int. J. Remote Sens. 19, 2223–2231.

Xu, H.Q., 2013. A remote sensing urban ecological index and its application. Acta Ecol. Sin. 33, 7853–7862 (In Chinese with English abstract).

Xu, H.Q., 2006. Modification of normalised difference water index (NDWI) to enhance open water features in remotely sensed imagery. Int. J. Remote Sens. 27, 3025–3033.

Xu, H.Q., 2008. A new index for delineating built-up land features in satellite imagery. Int. J. Remote Sens. 29, 4269–4276.

Xu, H.Q., Ding, F., Wen, X.L., 2009. Urban expansion and heat island dynamics in the Quanzhou region, China. IEEE J. Sel. Top. Appl. Earth Obs. Remote Sens. 2, 74–79.

Xu, H.Q., Huang, S.L., Zhang, T.J., 2013. Built-up land mapping capabilities of the aster and Landsat ETM+ sensors in coastal areas of southeastern China. Adv. Space Res. 52, 1437–1449.

Xu, H.Q., Zhang, T., 2013. Assessment of consistency in forest-dominated vegetation observations between aster and Landsat ETM+ images in subtropical coastal areas of Southeastern China. Agric. For. Meteorol. 168, 1–9.

Yang, Y., Wong, K.K.F., 2013. Spatial distribution of tourist flows to China's cities. Tourism Geographies: Int. J. Tourism Space Place Environ. 15, 338–363.

Yuan, F., Wu, J.G., Li, A., Rowe, H., Bai, Y.F., Huang, J.H., Han, X.G., 2015. Spatial patterns of soil nutrients, plant diversity, and aboveground biomass in the Inner Mongolia grassland: before and after a biodiversity removal experiment. Landscape Ecol. 30, 1737–1750.

Zawadzki, J., Cieszewski, C.J., Zasada, M., Lowe, R.C., 2005. Applying geostatistics for investigations of forest ecosystems using remote sensing imagery. Silva Fennica 39, 599–618.

Zawadzki, J., Fabijańczyk, P., 2013. Geostatistical evaluation of lead and zinc concentration in soils of an old mining area with complex land management. Int. J. Environ. Sci. Technol. 10, 729–742.

Zawadzki, J., Magiera, T., Fabijańczyk, P., 2009. Geostatistical evaluation of magnetic indicators of forest soil contamination with heavy metals. Stud. Geophys. Geod. 53, 133–149.

Zawadzki, J., Przeździecki, K., Miatkowski, Z., 2016. Determining the area of influence of depression cone in the vicinity of lignite mine by means of triangle method and Landsat TM/ETM+ satellite images. J. Environ. Manage. 166, 605–614.

Zhang, J.Q., Zhu, Y.Q., Fan, F.L., 2016. Mapping and evaluation of landscape ecological status using geographic indices extracted from remote sensing imagery of the Pearl River Delta, China, between 1998 and 2008. Environ. Earth Sci. 75, 327–342.

Zheng, B., Myint, S.W., Thenkabail, P.S., Aggarwal, R.M., 2015. A support vector machine to identify irrigated crop types using time-series Landsat NDVI data. Int. J. Appl. Earth Obs. Geoinf. 34, 103–112.